Geomorphology 497 (2026) 110178

Contents lists available at ScienceDirect

Geomorphology

journal homepage: www.journals.elsevier.com/geomorphology

Ongoing geological processes on the flanks of active volcanoes. A multi-scale geomorphological approach applied to the La Fossa Caldera (Vulcano Island, Italy)

Denise Petronelli [a], Claudia Romagnoli [b,c], Martina Pierdomenico [b], Alessandro Bosman [b], Francesco Latino Chiocci [a,b], Daniele Casalbore [a,b,*]

[a] DST, Department of Earth Sciences, University Sapienza of Rome, Italy
[b] CNR-IGAG, Institute of Environmental Geology and Geoengineering, National Research Council, Rome, Italy
[c] BiGeA, Department of Biological, Geological and Environmental Sciences, University of Bologna, Italy

ARTICLE INFO

Keywords:
Volcano
ROV exploration
Multibeam bathymetry
Bathymetric changes
Seafloor erosion
Caldera

ABSTRACT

The integrated analysis of successive multibeam bathymetry surveys and seafloor videos acquired from 2005 to 2023 provides crucial insights into the recent morphological evolution of the submerged part of La Fossa Caldera (Vulcano Island). The caldera floor is carved by a network of gullies and channels that often incise a coastal platform and submarine depositional terrace. Gullies are short (~15–430 m) and steep (~30°) erosional features characterized by their V-shaped cross-sections. In contrast, channels are relatively long (~350–1180 m) and flat-bottomed features. Channels show average slope gradients of ~15° and often host upper-flow regime bedforms along their thalweg, most of which have wavelengths of ~10–80 and heights of ~0.5–2 m. Despite the geologically-active setting of the study area, repeated multibeam surveys shows only minor morphological changes on the seafloor over the last 20 years. Seafloor erosion is dominant and often associated with small-scale retrogressive slope failures at the channel head, likely triggered by earthquakes or storm-waves that frequently hit the area. Seafloor erosion due to sediment-laden flows is observed offshore the Rio Grande creek, where coarse-grained deposits mixed with accumulation of plant debris are common. Small-scale rock-falls dominate the evolution of a steep escarpment that bounds the coastal platform, as testified by accumulation of squared metric blocks at their base. This study highlights the importance of multi-temporal and multi-scale geomorphological approaches to understand erosional processes that shape submarine volcanic flanks. Our results have key implications for geohazard assessments in such areas.

1. Introduction

Calderas are volcano-tectonic features developed both on subaerial and submarine volcanoes (Geyer and Marti, 2008). They are features that received recent attention due to their catastrophic eruptions, as witnessed by the recent Hunga Tonga 2022 tsunamigenic eruption (Lynett et al., 2022; Terry et al., 2022; Seabrook et al., 2023). Moreover, calderas are typically associated with hydrothermal systems of relevance to geothermal energy resources and ore deposits (Suárez-Arriaga et al., 2014; Rytuba, 1994). Thus far, little attention has been given to the erosional-depositional processes controlling the morphological evolution of calderas through time; yet, processes as these can generate local geohazards, especially if calderas are located in shallow water at or close to coastal communities. This is exactly the case of the La Fossa Caldera (LFC), part of the Vulcano Island in the Aeolian Archipelago, a UNESCO site attracting hundreds of thousands of visitors per year (Fig. 1). The LFC has been interpreted as a multi-stage caldera whose NE portion is submerged (De Astis et al., 2013). The caldera has been the site of intense volcanic activity in the last 5 ka, as proven by the formation of an active tuff cone (La Fossa Cone in Fig. 1b) that last erupted in 1888–1890 (Di Traglia et al., 2024). This tuff cone and the adjacent coastal area are affected by widespread degassing, with the most recent unrest episode occurring in 2021–2023 (Inguaggiato et al., 2022; Capecchiacci et al., 2025).

In this paper, we test a multi-temporal and multiscale geomorphological approach based on repeated multibeam bathymetric data and

* Corresponding author at: DST, Department of Earth Sciences, University Sapienza of Rome, Italy.
E-mail address: daniele.casalbore@uniroma1.it (D. Casalbore).

https://doi.org/10.1016/j.geomorph.2026.110178
Received 24 March 2025; Received in revised form 24 November 2025; Accepted 13 January 2026
Available online 15 January 2026

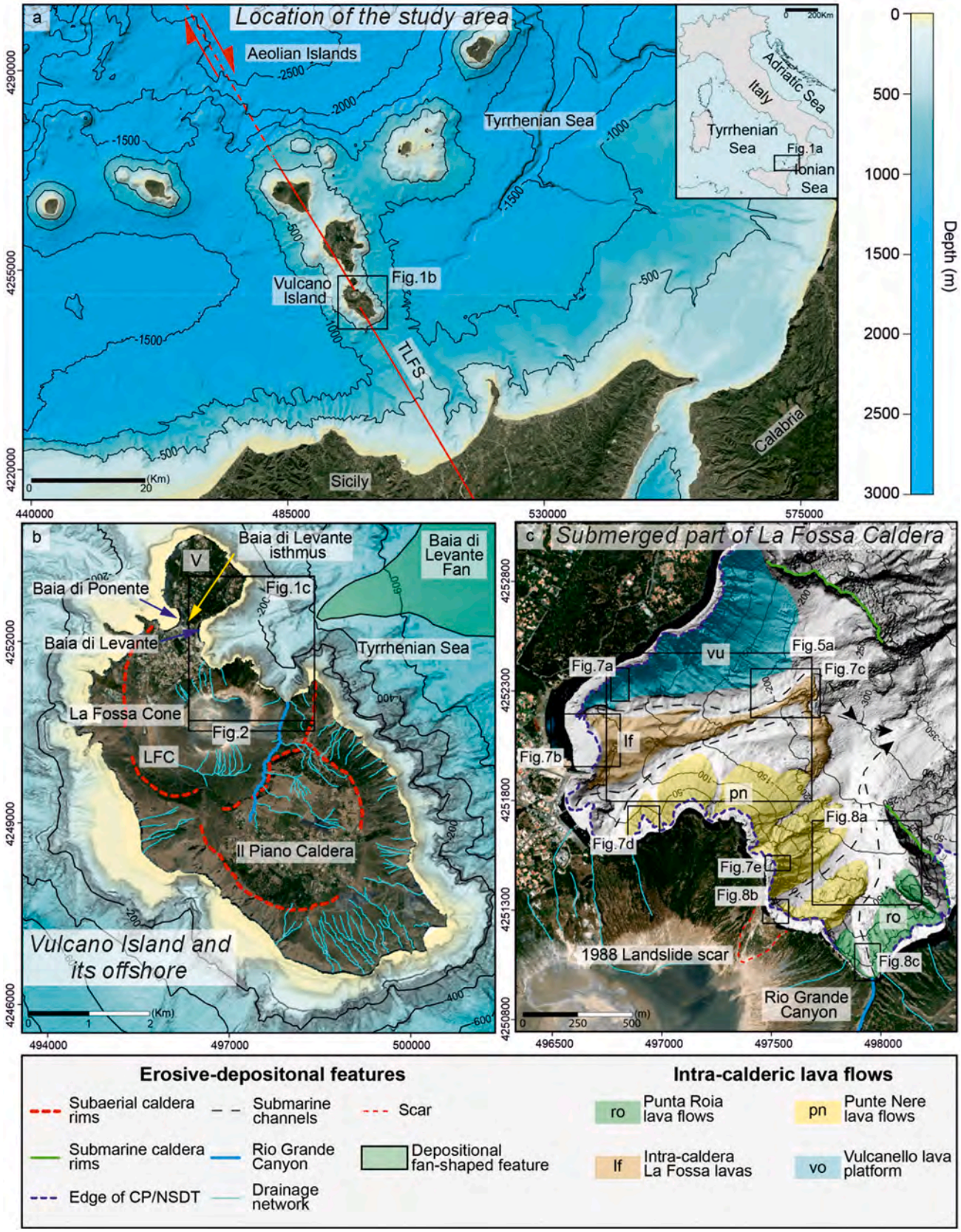

Fig. 1. a) Geographical location of Vulcano Island in the Southern Tyrrhenian Sea (bathymetry downloaded from http://www.emodnet-bathymetry.eu); TLFS: Tindari-Letojanni fault system from De Astis et al. (2023). b) Satellite image of Vulcano Island, with the trace of the caldera collapses and the subaerial drainage network, combined with the offshore bathymetry (isobaths every 200 m). V – Vulcanello; LFC – La Fossa Caldera. c) Zoom of the submerged part of the LFC (isobaths every 50 m), with the indication of the submarine rims, intra-calderic volcanic units and main erosional channels.
Modified from Romagnoli et al. (2012) and Casalbore et al. (2019).

video recordings from ROV/submersible dives, acquired over the last 20 years, to address the following questions:

1) What kind of erosional processes are affecting the morphological evolution of the LFC over the last 20 years?
2) What are the main factors controlling the formation of upper-flow regime bedforms within the submerged part of the LFC?
3) In what ways can these features be used in preliminary geohazard assessments of volcanic islands?

The latter issue is particularly relevant considering that, in case of a volcanic emergency, the main facility for the evacuation of the Vulcano Island is the Porto di Levante harbour (Ricciardi et al., 2024), located within the NE portion of the LFC near a submerged erosional feature (Fig. 2).

2. Geological setting

The Vulcano Island, located in the SE Tyrrhenian Sea, is the subaerial tip of a large volcanic complex that extends down to 1200 m below sea level (mbsl) (Fig. 1a). It is the southernmost edifice of the Aeolian volcanic arc, whose origin is related to the NW-directed subduction of the Ionian oceanic lithosphere below the Calabrian Arc (Gvirtzman and Nur, 1999; Ventura et al., 1999; De Astis et al., 2003). Together with the Lipari and Salina volcanic edifices, the island forms a NNW-SSE elongated volcanic belt controlled by a main strike-slip fault system, interpreted as the offshore prolongation of the regional Tindari–Letojanni tectonic system in Fig. 1a (Romagnoli et al., 2013; Ventura, 2013). Volcanic activity occurred on the island since 130 ka B.P. (De Astis et al., 2013).

Two calderas dominate the island's present-day topography (Fig. 1b): the older Il Piano Caldera (dated ≈100 ka) in the southern sector and the younger LFC in the northern sector. The LFC is a multi-phase and partially submerged caldera, formed by three main volcano-tectonic collapses ranging in time between ≈80 and ≈8.5 ka (De Astis et al., 2013; Casalbore et al., 2019). The most recent volcanic structures associated with the LFC are: a) the La Fossa Cone (Fig. 1b) emplaced in the central part of the caldera since ≈5.5 ka, and b) the Vulcanello lava platform (V in Fig. 1b) in the northern sector of the island (De Astis et al., 2013). Vulcano and Vulcanello are connected by an isthmus (Fig. 1b) formed by volcaniclastic sediment resulting from volcanic activity in the mid sixteenth century CE (Di Traglia et al., 2024). The flanks of the La Fossa Cone are made up of interbedded fine-grained and coarse-grained ashes, lava flows, and minor coarse-grained lapilli and bomb deposits, enabling the formation of low- and high-permeability levels (De Astis et al., 2013). During heavy rainfall events, the loose and more permeable lithologies are mobilized, creating small debris flows eroding the La Fossa Cone's ephemeral drainage network (Fig. 1b) (Ferrucci et al., 2005; Di Trapani et al., 2011; Bonasia et al., 2022). Erosional processes are also favoured by hydrothermal activity that hindered the

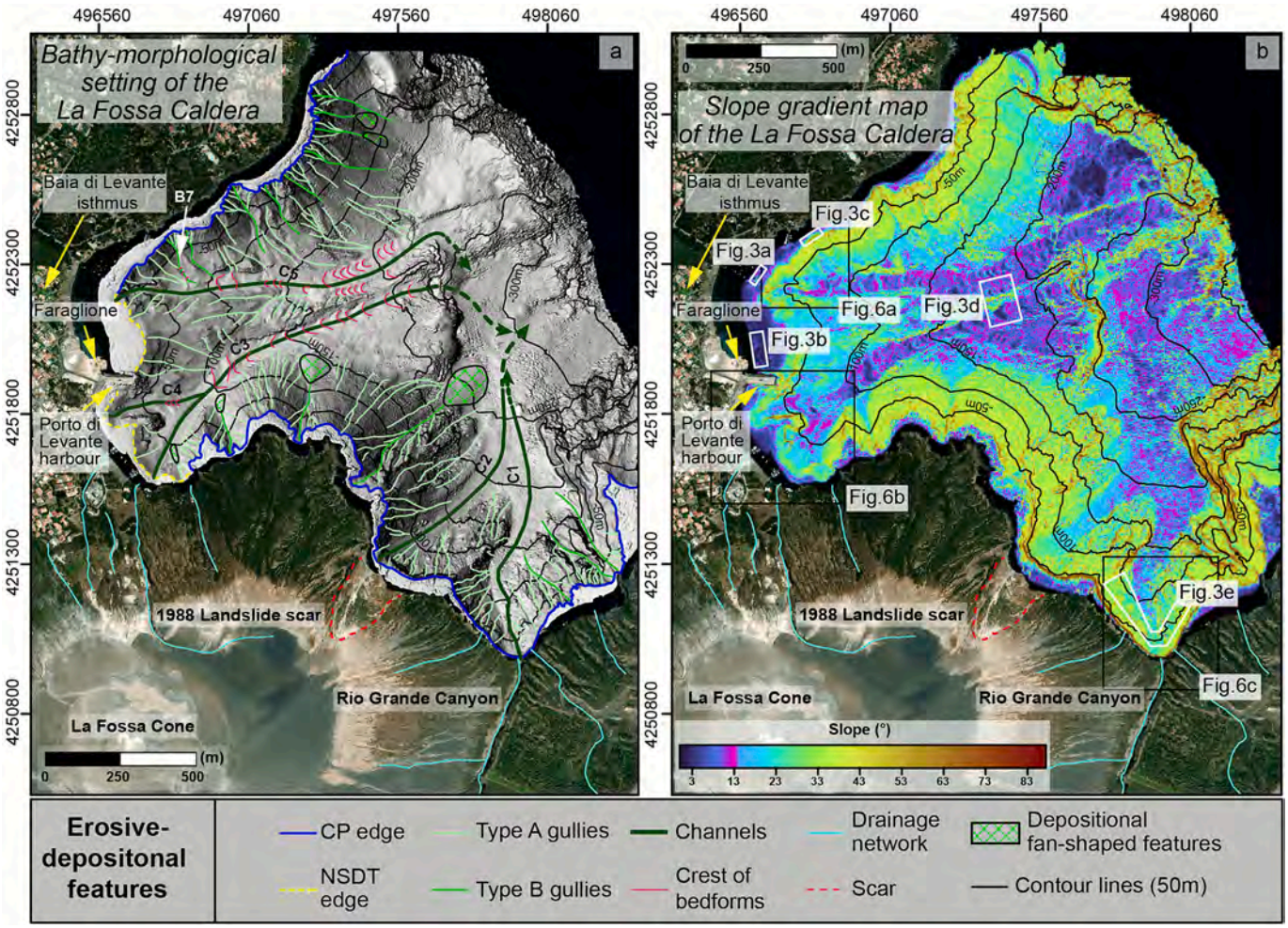

Fig. 2. a) Shaded relief map and isobaths (equidistance of 50 m) of the submerged portion of the LFC (location in Fig. 1b), with the mapped erosional-depositional features. b) Slope gradient map of the submerged portion of the LFC; the threshold slope value (13°) for the formation of bedforms is indicated by magenta colour (see text for detail).

development of vegetation (Madonia and Liotta, 2010). Small-scale slope failures can be also triggered by earthquakes that frequently affect the area (Agnesi et al., 2005; Falsaperla et al., 2025). As a result of all these processes, the eastern flank of La Fossa Cone is bounded by a narrow and short canyon (Rio Grande Canyon in Figs. 1b, c and 2a), hosting the main water course of Vulcano Island (Di Traglia et al., 2013).

The NE portion of the LFC is submerged at present, being partially bounded by two steep ridges (Figs. 1c and 2); they have been interpreted as the offshore extent of the subaerial caldera rims (Gabbianelli et al., 1991; Romagnoli et al., 2012). Casalbore et al. (2019) recognized a series of submarine geomorphic features that can be correlated with intracalderic volcanic units on land, such as: a) the submarine flank of the Vulcanello lava platform (vu in Fig. 1c, dated at 900–1050 CE by Malaguti et al., 2022), b) the submarine volcanic lobes of the Punte Nere lava flow unit (pn in Fig. 1c, dated between 3683 BCE and 1168 CE by Malaguti et al., 2022), and c) the submarine extent of the Punta Roia lava flow units (ro in Fig. 1c; dated at 14–13 ka by De Astis et al., 2013). A submarine volcanic ridge (If in Fig. 1c) is also observed between Punte Nere and Vulcanello, but its origin and age are still unknown. The shallow (< 20 m bsl) parts of these units are characterized by a coastal platform (CP in Fig. 1c and 2a), with the outer edge located at 5–12 mbsl. The CP edge is affected by small-scale landslide/erosional scars, representing the head of erosional features. These converge downward in a main valley that fed a large volcaniclastic fan outside the breached caldera border (Baia di Levante fan in Fig. 1b; Romagnoli et al., 2012). One of these erosional features is morphologically linked to a landslide scar formed in 1988 (red dashed line in Fig. 2b) located on the NE flank of La Fossa Cone, which mobilized ≈200,000 m^3 of material and produced small tsunami waves in the northern part of the island (Tinti et al., 1999).

2.1. Climatological and oceanographic settings

The meteo-marine regimes of the Aeolian Archipelago are dominated by NW and W winds (Cicala, 2000), leading to the formation of westerly storm-waves with a maximum significant wave height estimated around 3.5 m near the Lipari Island (Romagnoli et al., 2022). The Archipelago is secondarily impacted by SE and E storms with maximum wave heights around 2.5 m. Vulcano Island's climate exhibits typical semi-arid Mediterranean conditions with an average annual precipitation of only 615 mm (Di Trapani et al., 2011). Even so, the island is sporadically hit by heavy rain events, as revealed by the analysis of precipitations extracted from the nearest available meteorological station located at Salina Island (Bonasia et al., 2022; Fig. 1ESM). These events can trigger mud/debris flows from the La Fossa Cone to the surrounding plains, which often reach the coast, as lately occurred on 14 September 2008 (Bonasia et al., 2022).

3. Materials and methods

3.1. Multibeam bathymetry and backscatter data

Consecutive bathymetric surveys were carried out between 2003 and 2023 to map the submarine portion of LFC from the coastal sectors down to ≈320 mbsl. The first surveys occurred between 2003 and 2005 using multibeam systems working at frequencies from 455 kHz in the shallow sectors to 50–240 kHz at greater depths. Data were RTK- and DGPS-positioned for shallow- and deep-water surveys, respectively. In 2014, a new PPK-positioned bathymetric survey was performed in the first 150 mbsl onboard a small launch, using a multibeam system working at a frequency of 400 kHz (Bosman et al., 2015). The most recent bathymetric surveys were RTK-positioned and acquired in 2022 and 2023 between 5 and 320 mbsl using multibeam systems working at frequencies of 200–450 kHz. Patch tests, daily acquisition of sound velocity profiles and tidal data were applied to all the surveys. Multibeam data were gridded at a cell-size variable from 0.5 m in the first 100 m to 2 m at greater depths. For the 2022 and 2023 surveys, backscatter data were also processed, enabling the generation of a mosaic with a 0.5 m cell-size.

Bathymetric profiles performed on the Digital Elevation Models (DEMs) were used to extract the morphometric parameters of 207 erosional features, characterized by incision depths greater than 1 m with respect to their surroundings, and associated bedforms. Morphometric parameters for erosional features include length, incision depth, slope gradients and sinuosity index, i.e., the ratio between the along-channel distance and the straight-line distance of the channelized lineaments. For bedforms, the morphometric parameters include wavelength, wave height, average slope gradient, length and slope gradient of their stoss and lee sides. DEM of Difference (DoD) (Williams, 2012) was obtained by comparing successive bathymetries (2014 vs 2005, 2022 vs 2014, 2023 vs 2022) using Global Mapper 15. An overall vertical accuracy range of ±0.1 m was estimated for each DoD by comparing difference in depth of stable benchmarks between bathymetric sets. Depth changes below this error range in the DoD were not considered in volume estimates.

3.2. Video transects

The video records used in the study were collected at a depth range of 0.5–250 m during four oceanographic cruises carried out between 2020 and 2024. A total of 17 transects and ~ 13 h of video were acquired (Table 1). The analysis of the video sequences was aimed at the qualitative characterization of volcanic outcrops, seafloor textures and the identification of small-scale erosive-depositional features. Three video transects were acquired in 2020 by the GEOMAR submersible JAGO, which was equipped with multiple LED lights, Full-HD video camera, and Ultra-Short Base Line (USBL) positioning system. Twelve video transects were shot in 2022 and in 2023 using the Seamore Marine Steelhead ROV (Remotely Operated Vehicle), equipped with a standard definition camera, an auxiliary Full-HD video camera (GoPro), parallel green laser pointers for scale (with a laser distance of 10 cm), and a USBL system for the positioning of ROV tracks. The USBL system did not work in very shallow-water stations affected by degassing (ROV_01 and ROV_02). In such cases, the position was roughly estimated based on vessel position and morphological features visible on the DEMs. Finally, three video transects were acquired in 2024 using the ROV POLLUX III (ROV_13) and the EPRONS ROV D500 (ROV_14 and ROV_15). The ROV POLLUX III was equipped with both a digital and a high-definition camera, while the EPRONS ROV D500 was equipped with a 4K colour camera. In both cases, a USBL system was installed on the ROV and two parallel red lasers spaced 15 cm apart were used for scale. The USBL data from all surveys were post-processed to manually remove out-of-sequence beams, spikes, and to smooth the navigation tracks.

4. Results

The submerged portion of LFC is a depressed area of ~2 km^2 that extends down to ~320 mbsl (Figs. 1c and 2a). Shallow-water sectors (< 17 mbsl) are generally characterized by terraced features, i.e., coastal platform and nearshore submarine depositional terraces (CP and NSDT in Fig. 2a, respectively). The CP has an outer edge at 10–17 mbsl and a width (from the coast to the edge) variable from 5 to 90 m. Its slope gradients are 8°-15°, with a marked increase to values >40° beyond its edge (locally sub-vertical, Fig. 2b). The CP surface is rough due to accumulations of blocks and volcanic outcrops (BA and VO, respectively in Fig. 3a), which are typically characterized by high backscatter values. In a few sectors (as to the NW), the CP displays a smoother morphology and medium backscatter values in an area of sandy seafloor (SS in Fig. 3c). The NSDT is well recognizable in the central part of the bay, offshore the Baia di Levante isthmus (Fig. 2a); it is 210 m wide, with the outer edge located at 5–12 mbsl. The top of the NSDT has slope gradients <4°, increasing to 20°-30° beyond its edge (Fig. 2b). The NSDT shows a

Table 1
Location and characteristics of video transects collected between 2020 and 2024 by submarine and ROV. SoT and EoT: Start and End of the Transect; (*) ROV_01 and ROV_02 have not length because the USBL system didn't work in shallow water.

Cruise	Year	Track ID	Latitude (SoT)	Longitude (SoT)	Latitude (EoT)	Longitude (EoT)	Length (m)	Depth range (m)	
AL533	2020	JAGO_08	38°24′40.9″N	14°58′35.1″E	38°24′37.5″N	14°58′34.1″E	188	118	174
AL533	2020	JAGO_10	38°24′41.7″N	14°58′40.5″E	38°24′44.2″N	14°58′41.8″E	443	86	205
AL533	2020	JAGO_12	38°24′47.8′N	14°58′34.3″E	38°24′44.3″N	14°58′25.5″E	290	150	227
Vulcano 2022	2022	ROV_01	38°24′58.5″N	14°57′40.6″E	38°24′58.8″N	14°57′40.4″E	-*	0.8	6
Vulcano 2022	2022	ROV_02	38°25′03.3″N	14°57′37.5″E	38°25′03.3″N	14°57′37.5″E	-*	0.5	2.58
Vulcano 2022	2022	ROV_03	38°24′47.6″N	14°57′52.0″E	38°24′47.2″N	14°57′53.1″E	399	3.5	53
Vulcano 2022	2022	ROV_04	38°24′36.5″N	14°58′19.7″E	38°24′36.4″N	14°58′16.7″E	153	4.5	67
Vulcano 2022	2022	ROV_05	38°24′26.3″N	14°58′37.0″E	38°24′27.2″N	14°58′32.8″E	156	12	30
Vulcano 2023	2023	ROV_06	38°25′06.9″N	14°57′49.0″E	38°25′11.2″N	14°57′47.2″E	189	6	75
Vulcano 2023	2023	ROV_07	38°25′04.7″N	14°57′41.6″E	38°25′04.2″N	14°57′39.7″E	95	5	23
Vulcano 2023	2023	ROV_08	38°24′57.7″N	14°57′48.1″E	38°24′59.8″N	14°57′39.9″E	287	5	60
Vulcano 2023	2023	ROV_09	38°24′50.9″N	14°57′55.3″E	38°24′48.1″N	14°57′53.6″E	116	7	65
Vulcano 2023	2023	ROV_10	38°24′42.7″N	14°58′19.9″E	38°24′43.1″N	14°58′16.8″E	117	4	63
Vulcano 2023	2023	ROV_11	38°24′37.3″N	14°58′19.1″E	38°24′35.1″N	14°58′17.8″E	115	5.5	68
Vulcano 2023	2023	ROV_12	38°24′29.5″N	14°58′35.2″E	38°24′26.1″N	14°58′36.5″E	303	21	79
Vulcano 2024	2024	ROV_13	38°25′10.9″N	14°58′23.0″E	38°25′05.6″N	14°58′13.5″E	425	185	227
Vulcano 2024	2024	ROV_14	38°25′05.4″N	14°58′25.2″E	38°25′06.9″N	14°58′23.8″E	219	205	246
Vulcano 2024	2024	ROV_15	38°24′30.8″N	14°58′33.7″E	38°24′29.3″N	14°58′37.4″E	124	40	90

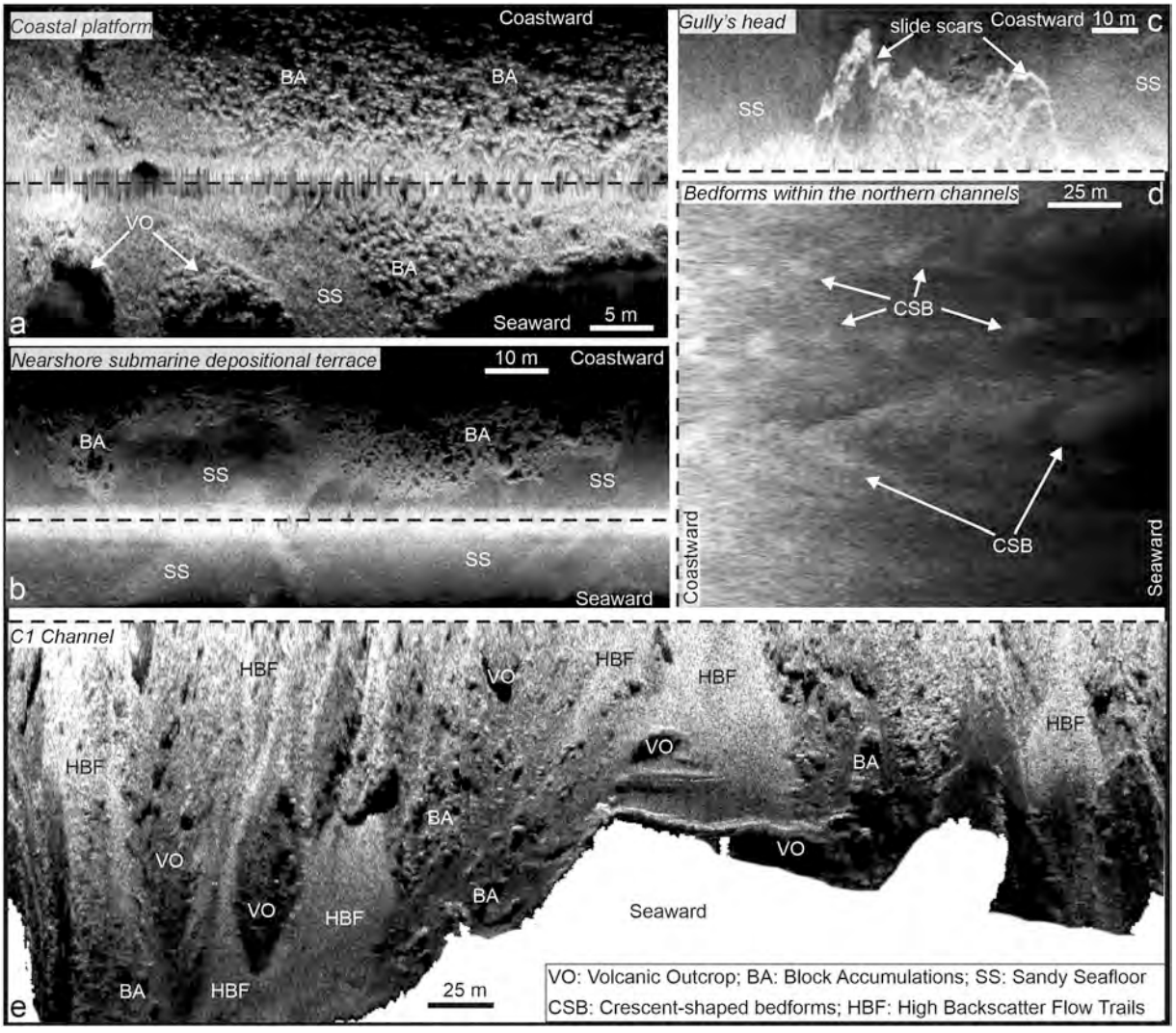

Fig. 3. Multibeam backscatter images (location in Fig. 2b), with light-tones corresponding to high-backscatter values. a) Blocky accumulations alternated with remnants of lava flows on the coastal platform; b) sandy seafloor on the top of the nearshore submarine depositional terrace, with local accumulation of blocks towards the coast; c) high-backscatter tones associated with the head of a gully; d) coaxial trains of crescent-shaped bedforms along the thalweg of the northern channels; e) upper reach of the southernmost C1 channel, where high-backscatter flow trails are alternated to volcanic outcrops and local accumulation of blocks.

smooth morphology and medium backscatter values due to its sandy seafloor (SS in Fig. 3b), except for occasional block accumulations near the coast (BA in Fig. 3b). Below the CP and NSDT edges, the volcanic flank is steep (Fig. 2b) and shows several erosional-depositional features (Fig. 2a and Section 4.1).

4.1. Channels, gullies and bedforms

The edges of the CP and NSDT are often incised by channels and gullies, which have steep heads (from 22° to 84°), with the higher slope gradients observed at the CP's edge. Gully's head (SGH in Fig. 3c) also shows higher backscatter values with respect to the surrounding areas. A total of 207 channels and gullies were identified in the study area (Fig. 2 and Table 2).

Gullies are steep, rectilinear features, with lengths from tens to some hundreds of meters (Fig. 2a and Table 2). They have straight or very slightly concave-upward longitudinal profiles (Fig. 4a, b). Based on their morphometric characteristics, gullies can be further divided into two sub-categories: Type A and Type B gullies.

Type A gullies are the shortest and shallowest features (Table 2), commonly characterized by their V-shaped cross-sections.

Type B gullies are characterized by their U- or V-shaped cross-sections in the upper reaches, locally becoming flat-bottomed with depths (Fig. 2). Knickpoints or trains of small-scale bedforms can occur along their thalweg (slope gully B7 in Figs. 2a and 4b), while small fan-shaped depositional features form at their base (Fig. 2a).

Channels are the longest erosional features recognized in the submerged part of the LFC (Table 2); they are located among main volcanic outcrops and extend over 300 mbsl. They have a slightly sinuous path in plan-view (Fig. 2) and show slightly concave-upward longitudinal profiles (Fig. 4c), with average slope gradients of ≈15° (Table 2). The southern channels C1 and C2 (Figs. 2a and 4c) are steeper than the northern channels C3–4 and C5. All of them converge downslope into a wide depression (Fig. 2a). Channels are flat-bottomed and show a relatively smooth morphology, with small-scale roughness occurring locally due to volcanic outcrops, sparse blocks and coaxial trains of bedforms (Figs. 2a and 5). They also show high-backscatter flow trails along their thalweg (HBF in Fig. 3e).

Coaxial trains of sinuous or crescent-shaped bedforms are present within the flat-bottomed channels located in the northern sector of the LFC (Figs. 4c and 5). They develop from 66 to 228 mbsl on slope gradients <13° (locally up to 15°), with wavelengths of 9–78 m and wave heights of 0.2–2.3 m (Table 3). The cross-sectional shape of the bedforms is downslope asymmetric, with a longer and gently sloping stoss side followed by a shorter and steeper lee side (Fig. 5 and Table 3). Based on their location and morphometric parameters, three bedform fields have been identified in the channels (Fig. 5 and Table 3). Bedforms generally show low-backscatter on the stoss side and high-backscatter at the crest and lee side (Fig. 3d).

4.2. Morphological changes between 2005 and 2023

The comparison of consecutive multibeam surveys in the submerged part of the LFC has shown small seafloor changes in three different areas over the last 20 years, especially when considering the 2005–2014 period (Fig. 6).

The first area is located offshore the Vulcanello lava platform, where the 2014–2005 DoD shows the occurrence of retrogressive (coastward) erosion at the B7 gully head, with a maximum mobilized thickness of 5 m (profile 1 in Fig. 6). Minor erosion (up to 1 m in thickness) also occurs along the thalweg of this gully and is associated with the formation of a train of crescent-shape bedforms (profile 2 in Fig. 6). Only in the distal part, the B7 gully shows erosion alternated with seafloor accretion (Fig. 6b).

The second area is located southward of the Porto di Levante harbour, where the 2014–2005 DoD (Fig. 6d) shows minor seafloor erosion both at the head of the C3 channel and along the thalweg of the C3 and C4 channels, associated with the migration of small-scale bedforms (Fig. 6c and profiles 3 and 4). Minor slope accretion occurs in the upper reach of the C3 channel (Fig. 6d), resulting in a slight progradation of the NSDT edge.

The third area is located offshore the Rio Grande Canyon, where the 2014–2005 DoD shows a marked seafloor erosion of the C1 channel's thalweg over an area of ≈5,000 m^2 down to 100 mbsl, with thickness of remobilized sediment up to 6 m, for an estimated volume of ≈17,000 m^3 (Fig. 6f and profile 6). Comparison between the 2014 and 2023 bathymetry reveals further thalweg erosion, especially along the eastern side of the C1 upper reach (profile 6 in Fig. 6). The head of the C1 channel also shows severe undercutting at its base, up to 6 m as recognizable in profile 5 of Fig. 6. Seafloor accretion is locally observed along the C1 thalweg (Fig. 6f), with the highest values due to the emplacement of large blocks (Fig. 6e), having a diameter around 10 m.

4.3. ROV and submersible video recordings

Three main seafloor types are observed in the video recordings: outcropping or sub-outcropping rocks, sandy/gravelly sediment, block accumulations (Figs. 7 and 8).

Outcropping/sub-outcropping rocks are observed near the coast down to 205 mbsl. They mainly occur on the coastal platform (Figs. 7d, e and 8b), often in relation to lobate volcanic outcrops made up of massive or fractured lava covered by algal turf (Fig. 9a). This seafloor type also characterizes sub-vertical escarpments bounding seaward the CP and NSDT (Figs. 7b, and 8b, c) as well as the base of the main volcanic outcrops (Figs. 7c and 8a). Escarpments are typically made up by brecciated or massive lava flows alternated with volcaniclastic layers, and locally show undercutting at their base (Fig. 9b).

Sandy/gravelly seafloor is mainly observed on the top of NSDT (Fig. 7b) and in the northern coastal platform (Fig. 7a), often arranged to form small-scale wavy bedforms (Fig. 9c, d) as well as along the thalweg of slope gullies and channels (orange line in Figs. 7a, c and 8a, c) with an overall decrease in grain size from shallow (Fig. 9e, i, j) to the deeper sectors (Fig. 9f). Based on qualitative observations, the dominant sediment fraction is volcaniclastic, with a minor content of bioclastic sediment. Gravelly deposits are mostly confined to the upper reach of channels C1 and C2 in the southern sector of the LFC (blue line in Fig. 8b, c), where they often form narrow and lobate deposits elongated along the maximum slope direction (Fig. 9e).

Block accumulations due to mass-wasting processes are observed at the base of the escarpments bounding volcanic outcrops as a debris cone (Figs. 7b, d and 8a, b); they also occur at the base of channels (Figs. 7c and 8a) and as isolated or scattered blocks along the thalweg of gullies and channels down to 250 mbsl (Figs. 7a, c and 8). Typically, the blocks have sub-metric or metric size and are from angular to sub-angular in

Table 2
Morphometric parameter of the channelized features; SI: sinuosity index.

Gullies and channels	Length (m)			Incision depth (m)			Slope gradients (°)			SI		
	Min	Max	Mean	Min	Max	Mean	Min	Max	Mean	Min	Max	Mean
Type A gullies (187)	16	415	97	1	15	2.8	13	58	30	1.00	1.13	1.03
Type B gullies (15)	152	427	240	2	12	5.6	21	32	26.6	1.01	1.10	1.03
Channels (5)	349	1177	870	10	13	11.5	11	18	14.9	1.02	1.09	1.05

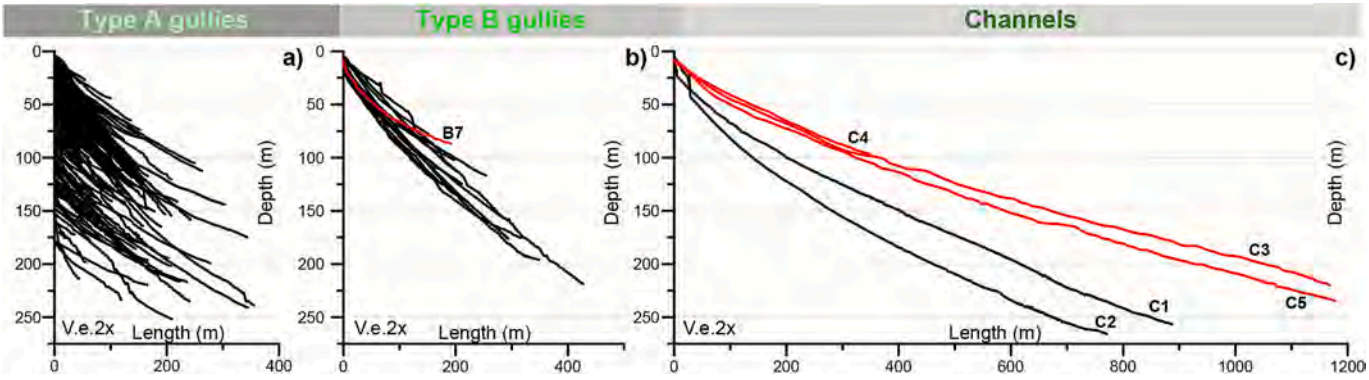

Fig. 4. Longitudinal profiles of the channels and gullies mapped in Fig. 2); V.e.: vertical exaggeration. The red profiles indicate the features with bedforms, corresponding to the northern channels C3–4 and C5 in Fig. 2a.

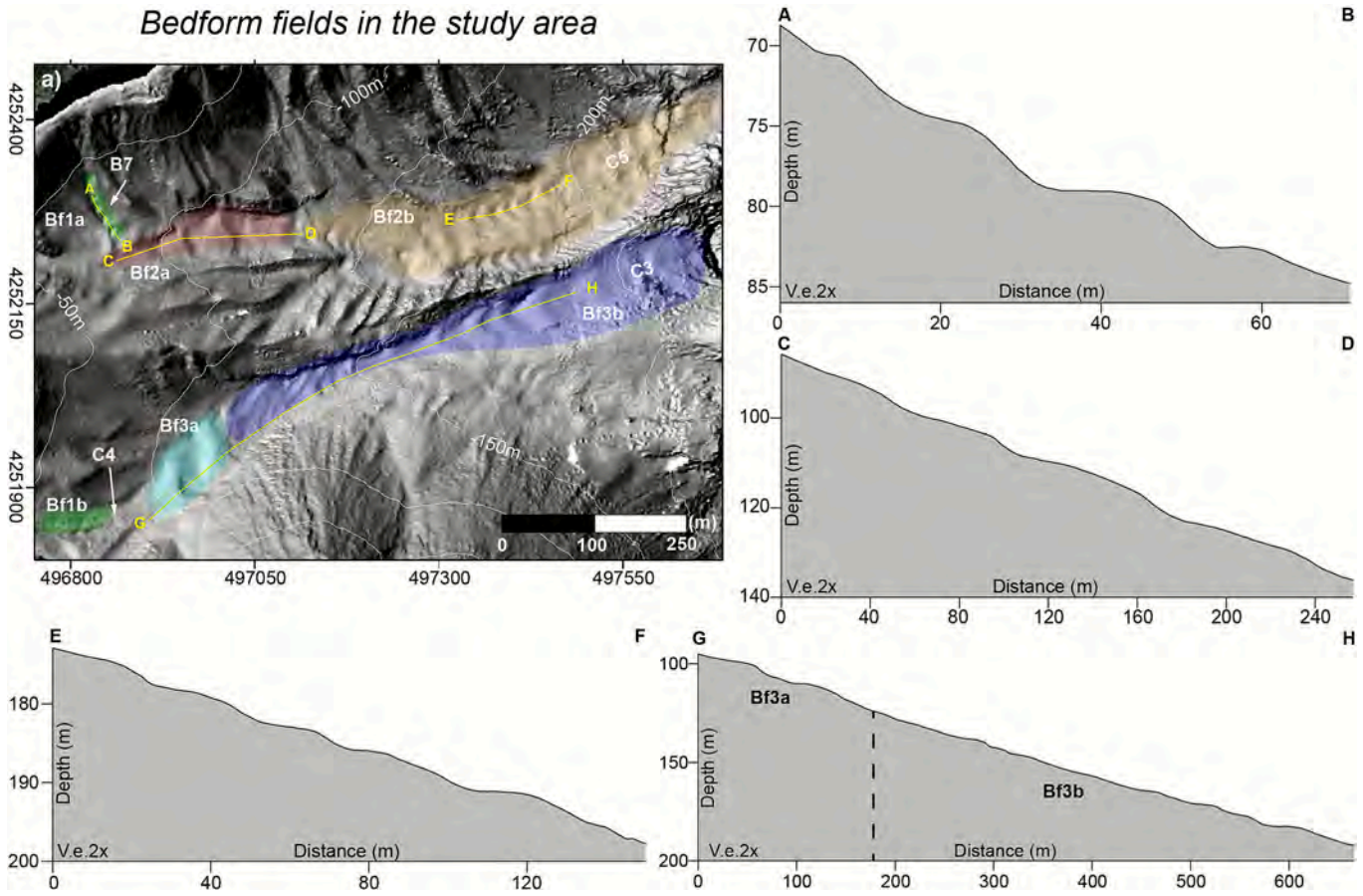

Fig. 5. a) Main bedform fields identified in the northern part of the La Fossa Caldera (Fig. 1c for location). Yellow lines are the trace of bathymetric profiles performed along the bedform fields. Note that vertical exaggeration (V.e.) is 2× for all profiles, but horizontal and vertical scale are different.

Table 3
Main morphometric characteristics of the bedform fields identified in the study area (for location see Fig. 5); slope gradients are represented as an average value.

Bedform field	Depth range (m)	Slope gradient (°)	Wave length (m)	Wave height (m)	Lee side length (m)	Stoss side length (m)	Lee side slope (°)	Stoss side slope (°)
Bf1a	68–84	12	9–21	0.5–1.3	4–11	3–9	20	3
Bf1b	66–79	13	14–19	0.4–0.5	3–9	6–12	18	9
Bf2a	85–136	11	34–67	0.9–1.8	12–24	14–46	19	9
Bf2b	135–228	8	12–35	0.2–1.2	5–21	2–22	13	4
Bf3a	94–116	9	51–67	1.6–2.3	13–24	29–43	17	4
Bf3b	116–210	8	9–78	0.3–2.2	3–51	6–27	14	5

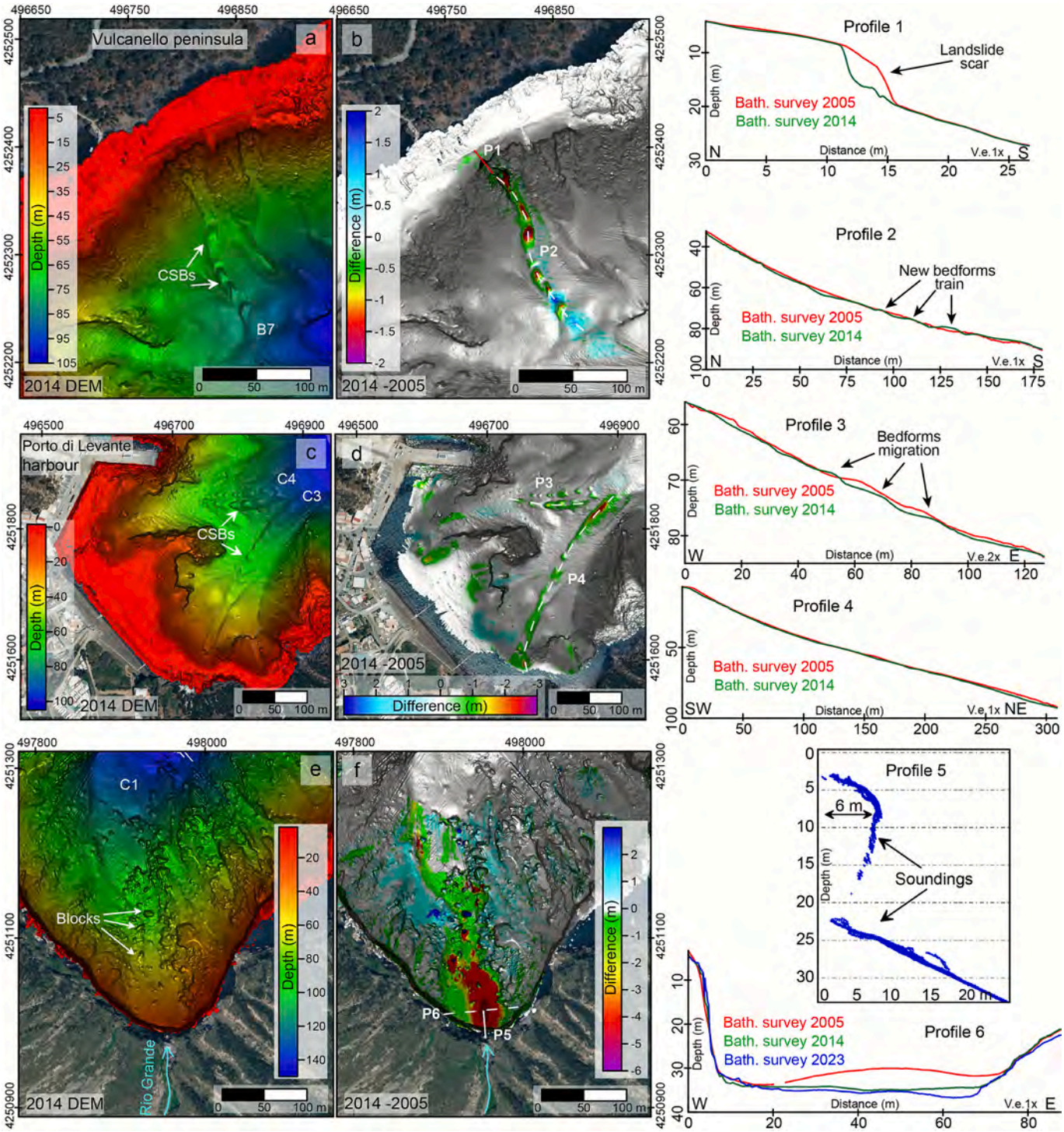

Fig. 6. (a, c, e) Shaded relief map of the 2014 bathymetry and (b, d, f) 2014–2005 DoD draped over the 2014 bathymetry for the B7 gully off Vulcanello, C3 and C4 channels off the Porto di Levante harbour, and C1 channel off Rio Grande Canyon, respectively; for location see Fig. 2. On the right, bathymetric profiles show seafloor variations occurred between 2005, 2014 and 2023 (the latter only for the C1 channel) bathymetries. Profile 5 shows the soundings collected during the 2023 survey, evidencing severe undercutting (up to 6 m) at the base of the escarpment bounding seaward the coastal platform.

shape, witnessing limited transport (Fig. 9g, h). In some areas, blocks are characterized by white, orange/red and violet colours, suggesting hydrothermal alteration. Generally, they show poor or no sedimentary cover; only in correspondence of some gullies (i.e., gully B7 in Fig. 2), blocks are partially buried in the seafloor. Accumulations of rounded blocks are locally found in the nearshore areas on the top of CP and NSDT (Fig. 7b, d).

Hints on depositional processes are provided by the distribution of plant debris on the seafloor observed in the videos. Accumulations of seagrass leaves (Fig. 9i) and terrestrial plant debris (Fig. 9e, j) occur within the thalweg of gullies and channels down to 200 mbsl (Figs. 7 and 8). Seagrass was observed forming compact meadows on the CP and NSDT (at <15 mbsl). Terrestrial plant debris is mostly observed along the C1 channel, offshore the Rio Grande Canyon (ROV_05 and ROV_12 in Fig. 8c). It consists of small (1–2 m long) tree branches, lying on the seafloor or partially buried within sediment.

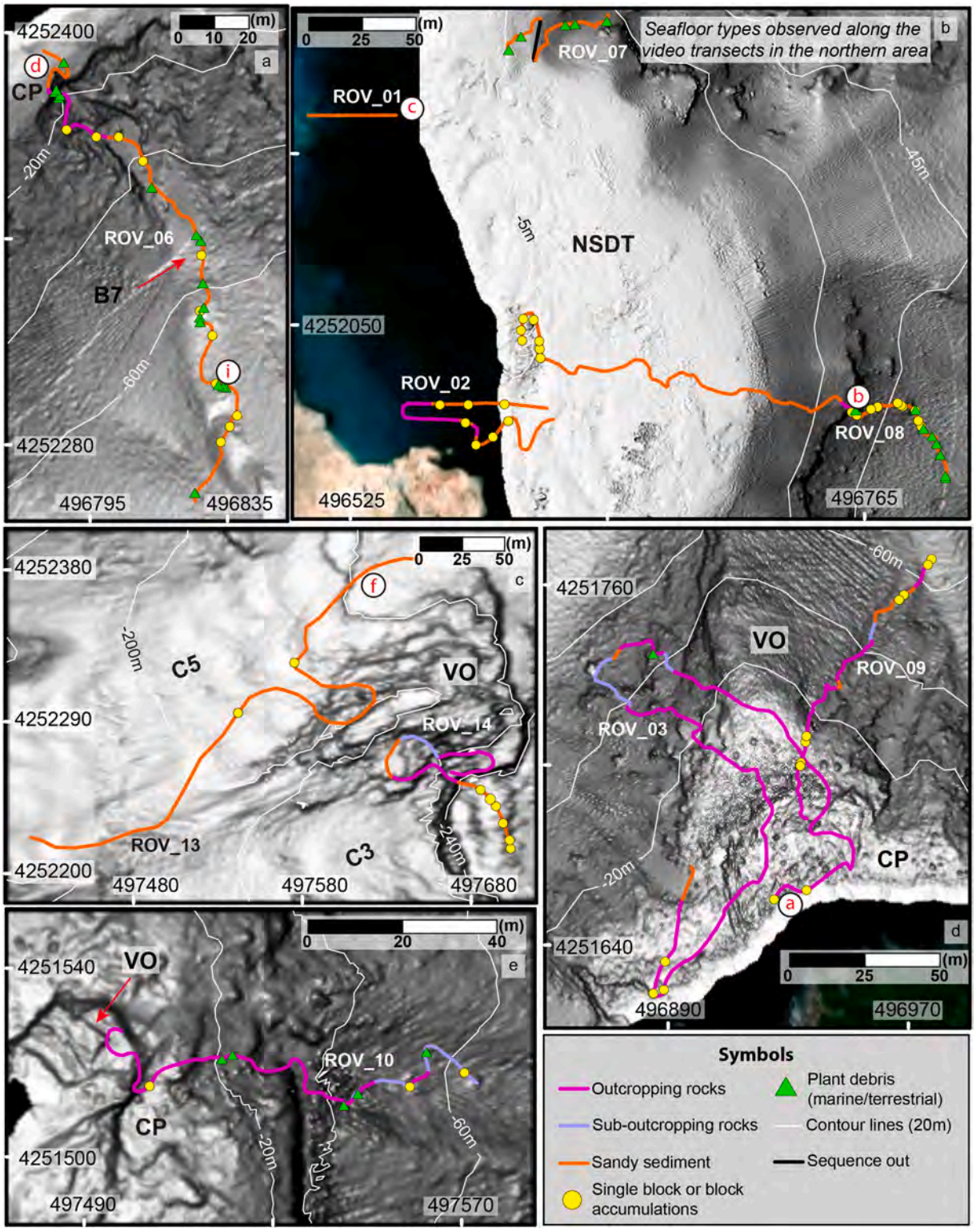

Fig. 7. Shaded relief map and contours (equidistance of 20 m; see Fig. 1c for location), with the seafloor types mapped along the ROV/submersible transects. The white circles with letters indicate the location of the images shown in Fig. 9. Acronyms as in the previous figures.

5. Discussion

5.1. Erosional processes within the submerged portion of La Fossa Caldera

Gullies and channels are due to the interplay between sediment-laden flows and marine retrogressive activity, as witnessed by comparison of consecutive multibeam surveys integrated by video observations (Figs. 6 and 9). The marked seafloor erosion occurred between 2005 and 2014 along the C1 channel (Fig. 6f) can be related to flash-flood generated hyperpycnal flows from the Rio Grande creek. These events are likely triggered by heavy rainfall events, as those recorded in 2005 and 2011 by the rain-gauge station located in the nearby Salina Island (Fig. 1ESM). This interpretation is also supported by the presence of flood deposits along the C1 thalweg, such as downslope elongated,

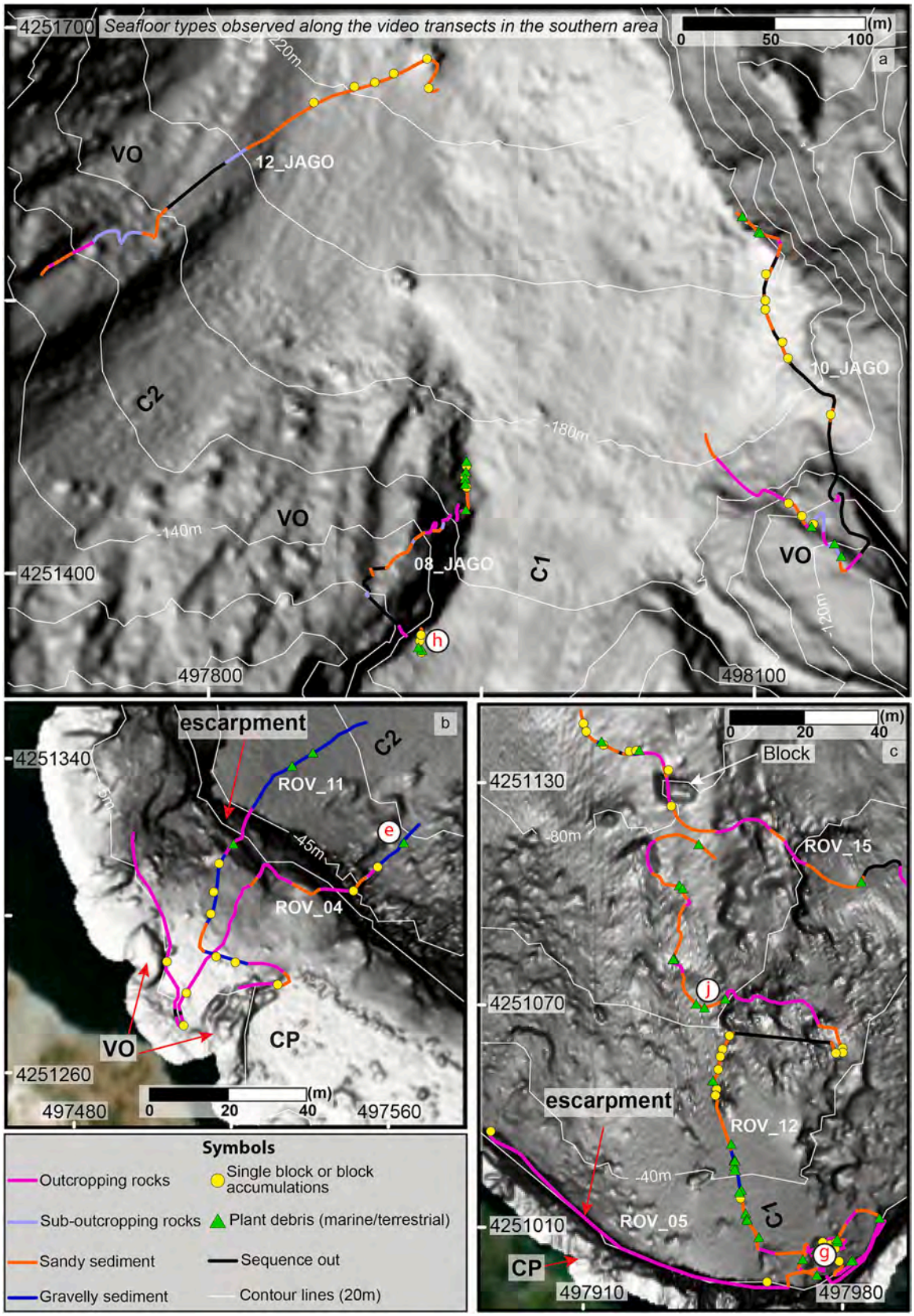

Fig. 8. Shaded relief map and contours (equidistance of 20 m; see Fig. 1c for location), with the seafloor types mapped along the ROV/submersible transects. The white circles with letters indicate the location of the images shown in Fig. 9. Acronyms as in the previous figures.

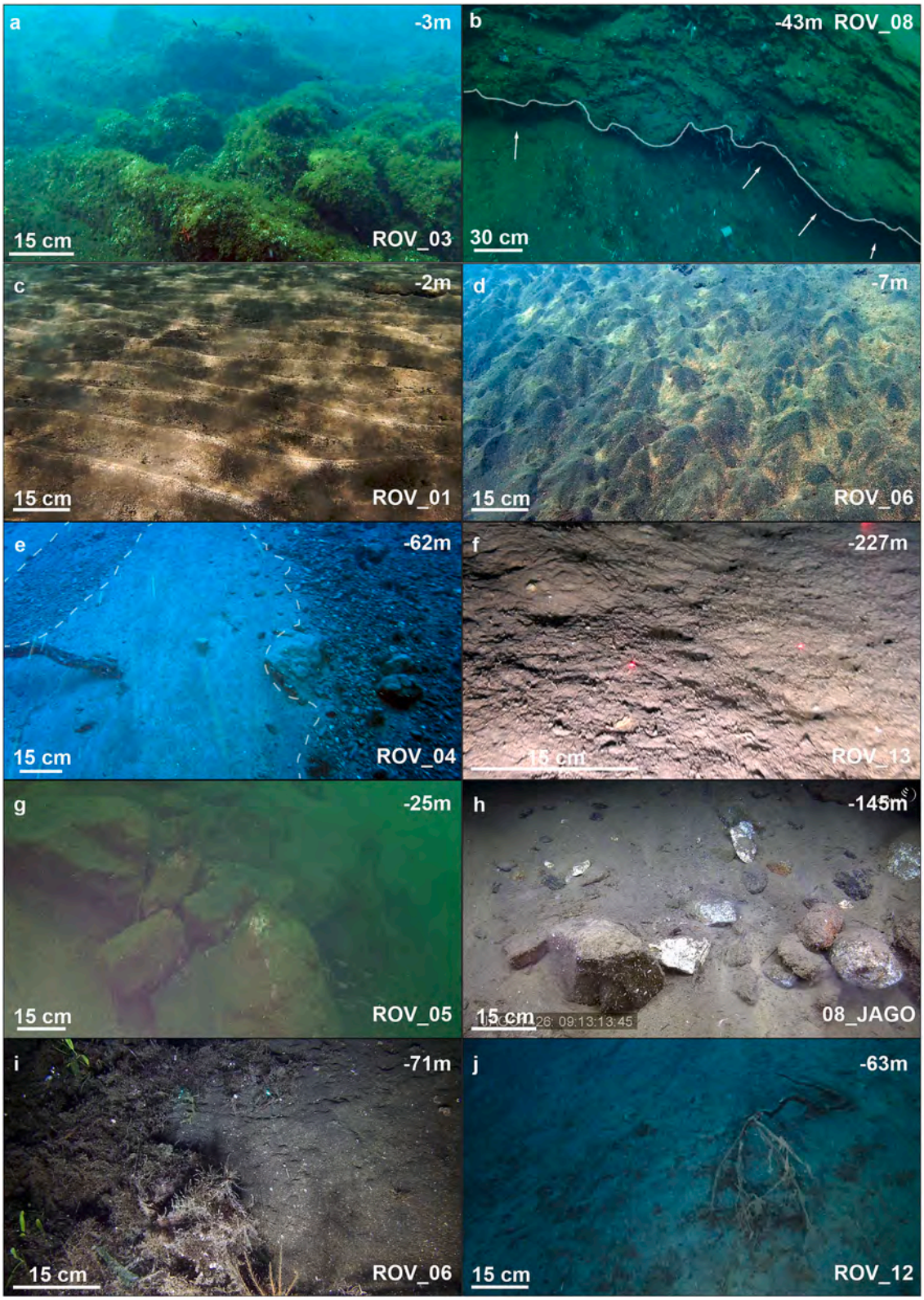

Fig. 9. Examples of seafloor types observed in the study area; location in Figs. 7 and 8. a) Algal turf that covers a rough rocky morphology on coastal platform; b) evidence of undercutting at the base of the scarps; c) megaripple field in sandy sediment on the nearshore submarine depositional terrace; d) sandy sediment with bioturbation on the coastal platform, e) fan-shaped gravelly deposits alternated with sandy seafloor and partially buried terrestrial plant debris along the C2 channel; f) silty sand in the distal reach of the C2 channel; g) blocks with poor sedimentary cover at the base of the escarpment bounding seaward the southern coastal platform; h) debris talus along the C1 channel with altered (likely hydrothermalized) blocks; i) sandy sediment with plant debris present along the gully B7; j) sandy sediment with small tree branches along the C1 channel, just off the Rio Grande Canyon mouth.

coarse-grained deposits along with accumulations of terrestrial plant debris (Fig. 9e, j). Sediment-laden flows due to small retrogressive slope failures are instead observed at the head of the B7 gully (Fig. 6a, b) and C3 channel (Fig. 6c, d). They could have been triggered by wave action, considering the shallow depth of their edge (around 10 mbsl), or possibly by the M4.6-earthquake occurred in August 2010, which also caused small landslides and rockfalls along the Vulcano and Lipari coastlines (Gambino et al., 2014). Seafloor erosion at the head of the C4 channel, located in the proximity of the Porto di Levante harbour, might have been also enhanced by anthropogenic effects due to the propellers of the daily ferries connecting the Aeolian Islands, similarly to what was reported for the Lipari harbour (Anzidei et al., 2016).

At LFC, the spatial distribution of gullies and channels has been controlled by volcanic activity over the last 14 ka (Casalbore et al., 2019; Fig. 1c). Narrow and mostly V-shaped gullies erode volcanic outcrops, while relatively wide and flat-bottomed channels are bounded by the main volcanic units (Figs. 1c and 2). Gullies and channels have also different longitudinal profiles (Fig. 4), likely reflecting their different location and morphological evolution, even if both features have not reached yet a final equilibrium profile (Mitchell, 2005; Soutter et al., 2021).

Rockfalls along steep escarpments cut on lavas and volcaniclastics are testified by the accumulation of polygonal blocks at their base and in surrounding areas (Fig. 9g, h). The recent occurrence of such processes is testified by the emplacement of large blocks between 2005 and 2014 along the C1 channel (Fig. 6e, f) that can be related to mass-wasting processes affecting the steep escarpment bounding the coastal platform here present. The rockfalls can be favoured by undercutting at the base of the escarpment, as evidenced by bathymetric profiles (profile 5 in Fig. 6) and seafloor videos (Fig. 9b). Nearshore undercutting processes in rocky coasts have been commonly related to wave action (e.g., Sunamura, 2021 and reference therein), but considering the depth range (30–50 mbsl) where they are recognized at the LFC, and the sheltered setting of this area from the main high-energy westerly storms, we suggest a main role of marine retrogressive erosion at the head of gullies/channels. Despite ROV dives did not reveal active seepage from the seafloor in this area, we cannot exclude a potential contribution on rocks alteration from hydrothermal activity. The NE subaerial flank of the La Fossa Cone is, in fact, characterized by active fumaroles that favour the occurrence of shallow mass-wasting processes (Madonia et al., 2019).

5.2. *Factors controlling the development of upper-flow regime bedforms within the channels*

Crescent-shaped bedforms recognized in the study area are generated by sediment-laden flows under supercritical flow conditions, based on their similarity in size (Fig. 10), plan-view geometry and cross-sections (Fig. 5) with upper-flow regime bedforms identified along the submarine flanks of insular volcanoes (Babonneau et al., 2013; Casalbore et al., 2021; Chang et al., 2022), as well as through flume experiments and numerical modelling (Cartigny et al., 2011; Slootman and Cartigny, 2020). In the submerged part of the LFC, upper-flow regime bedforms develop only along the thalweg of the northern channels (Fig. 2) and this is likely due to two main controlling factors: slope

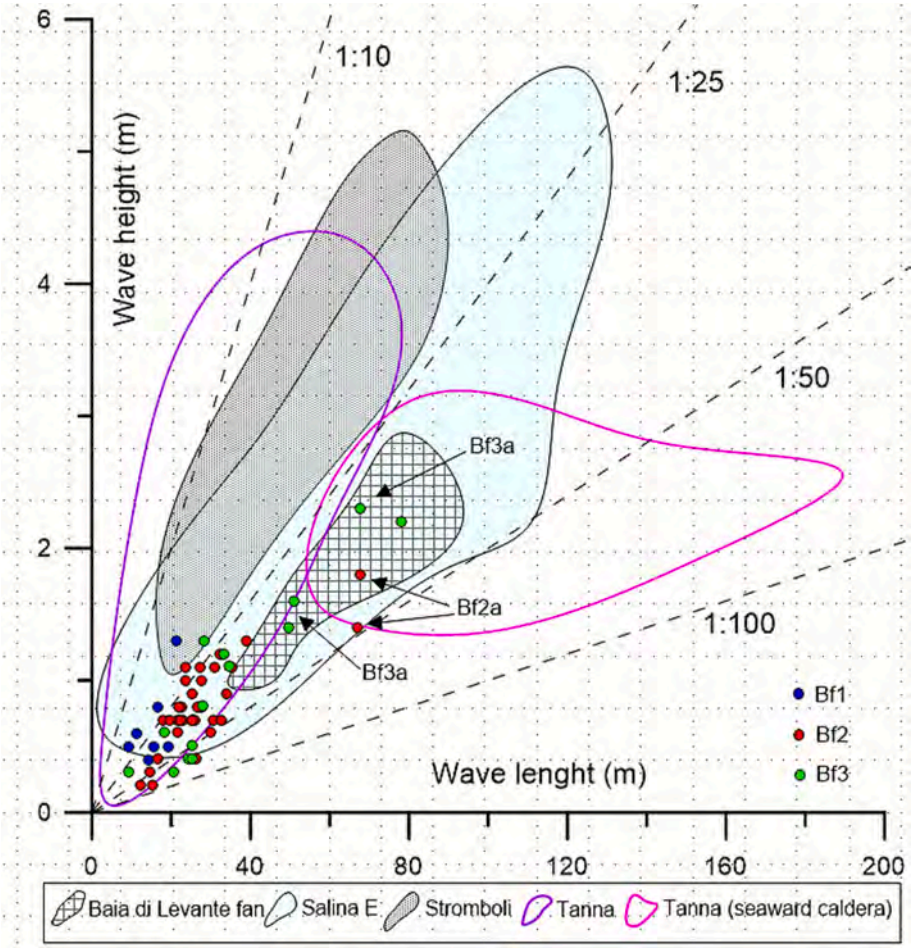

Fig. 10. Plot of wave height versus wavelength for all the recognized bedforms in the La Fossa Caldera and their comparison with similar features identified in the offshore Baia di Levante fan (see Fig. 1 for location), in the nearby Salina and Stromboli Islands, and offshore Tanna Island in the Vanuatu archipelago; data from Casalbore et al. (2021).

gradients and sediment grain-size. A maximum slope gradient of 13° was observed for the formation of the bedforms at the LFC, similarly to what reported in other submarine volcanic settings (Casalbore et al., 2021). Steeper declivities are commonly associated with fully-erosional sediment-laden flows (e.g., Clare et al., 2023), as testified by V-shaped cross-section of gullies in the study area (Figs. 2 and 4). Regarding sediment grain-size, a sandy seafloor is observed along the northern channels, because they are eroding the edge of a nearshore submarine depositional terrace, which is interpreted as a sand-rich prograding wedge (Casalbore et al., 2017; Figs. 7b and 9c). In contrast, the upper reaches of the southern channels (especially C2) are also floored by blocky and gravelly deposits due to the erosion of a sediment-starved coastal platform (Figs. 8b, c, and 9e, g), thus hindering the formation of upper-flow regime bedforms.

At the LFC, the recent formation of upper-flow regime bedforms is related to sediment-laden flows generated by minor retrogressive failures at the head of gullies and channels (Fig. 6a–d). These small-scale bedforms share a similar wave height – wave length ratio (H/L of 1:25 in Fig. 10), except for the largest ones found in the northern channels (Bf2a and Bf3a in Figs. 5 and 10). These latter could be the result of higher-magnitude flows, as also suggested by their fit with the parametric field of the bedforms found on the offshore Baia di Levante fan (Figs. 1b and 10).

5.3. *Implications for geohazard assessment and final remarks*

Minor seafloor erosion occurred in the submerged part of the LFC over the last 20 years (Fig. 6), mainly due to local retrogressive slope failures and related sediment-laden gravity flows. This morphological evolution is different from what observed in other very active volcanic settings, such as the nearby Stromboli Island (e.g., Casalbore et al., 2020, 2022, 2025; Di Traglia et al., 2022). The occurrence of limited erosion, as resulting by comparison among consecutive surveys, is a quite surprising finding considering the well-developed submarine drainage network of gullies and channels and the multiple predisposing/triggering factors for mass-wasting processes in the study area, including: a) persistent degassing activity, with the last volcanic unrest phase occurred in 2021–2023 (Federico et al., 2023; Capecchiacci et al., 2025), b) deep-seated deformations along the NE sector of the La Fossa Cone (Tommasi et al., 2007), and c) frequent and strong seismicity in the area (De Astis et al., 2023). On the other hand, the progressive retrogressive slope failures at the head of gullies and channels have implications for geohazard issues, because the Porto di Levante harbour represents the main evacuation gate for inhabitants and tourists in case of eruptive crisis (Ricciardi et al., 2024). So far, the morpho-bathymetric monitoring over the last 20 years did not evidence relevant seafloor changes around this harbour. However, we stress the importance of carefully monitoring its evolution in the future due to its strategic importance and the active geological dynamics present in the area. More generally, this study highlights the importance of a multi-scale geomorphological approach to better constrain the recent most evolution of geologically-active areas.

CRediT authorship contribution statement

Denise Petronelli: Writing – original draft, Visualization, Investigation, Data curation. **Claudia Romagnoli:** Writing – original draft, Investigation, Conceptualization. **Martina Pierdomenico:** Writing – review & editing, Methodology, Investigation. **Alessandro Bosman:** Writing – review & editing, Visualization, Methodology, Investigation. **Francesco Latino Chiocci:** Writing – review & editing. **Daniele Casalbore:** Writing – original draft, Visualization, Methodology, Investigation, Data curation, Conceptualization.

Declaration of competing interest

The authors declare that they have no known competing financial interests or personal relationships that could have appeared to influence the work reported in this paper.

Acknowledgements

We acknowledge Ministero dell'Ambiente e della Tutela del Territorio e del Mare-Geoportale Nazionale with license Creative Commons 3.0 Italy (CC BY-SA-3.0IT) for providing the high-resolution terrestrial Digital Elevation Model from Laser Imaging Detection and Ranging technology. We also acknowledge all colleagues, students and crews of the CNR Research vessels, Coastal Consulting & Exploration and Idrosfera that participated to the data collection. A special thank is due to the GEOMAR JAGO team for providing seafloor images of submersible dives performed in 2020 RV ALKOR Fahrtbericht Cruise (Report AL533; Hissmann et al., 2020). This research has benefited the support from the following projects: GNV-DPC funded projects: "The submarine portions of Italian volcanoes: their survey and assessment of the potential volcanic hazard" and "Study of the submerged structure of Vulcano and implications for risk assessment"; Accordo tra IGAG-CNR e Presidenza del Consiglio dei Ministri - Dipartimento della Protezione Civile 2019-2022 and 2022–2024; Progetto di Ateneo Medio 2021 and 2022, Sapienza University of Rome, P.I. Daniele Casalbore. We also highlight that the contents of this paper represent the authors' ideas and do not necessarily correspond to the official opinion and policies of Presidenza del Consiglio dei Ministri - Dipartimento della Protezione Civile. Finally, we gratefully acknowledge Andrew Gase, Tiago M. Alves and Dave Tappin for their comments on a previous version of the manuscript.

Appendix A. Supplementary data

Supplementary data to this article can be found online at https://doi.org/10.1016/j.geomorph.2026.110178.

Data availability

The data presented in this study are available on request from the corresponding author. The data are not publicly available due to their acquisition for institutional purposes.

References

Agnesi, V., Camarda, M., Conoscenti, C., Di Maggio, C., Diliberto, I.S., Madonia, P., Rotigliano, E., 2005. A multidisciplinary approach to the evaluation of the mechanism that triggered the Cerda landslide (Sicily, Italy). Geomorphology 65 (1–2), 101–116.

Anzidei, M., Bosman, A., Casalbore, D., Tusa, S., La Rocca, R., 2016. New insights on the subsidence of Lipari island (Aeolian islands, southern Italy) from the submerged Roman age pier at Marina Lunga. Quat. Int. 401, 162–173.

Babonneau, N., Delacourt, C., Cancouët, R., Sisavath, E., Bachèlery, P., Mazuel, A., Jorry, S.J., Deschamps, A., Ammann, J., Villeneuve, N., 2013. Direct sediment transfer from land to deep-sea: insights into shallow multibeam bathymetry at La Réunion Island. Mar. Geol. 346, 47–57.

Bonasia, R., Turchi, A., Madonia, P., Fornaciai, A., Favalli, M., Gioia, A., Di Traglia, F., 2022. Modelling erosion and floods in volcanic environment: the case study of the island of Vulcano (Aeolian Archipelago, Italy). Sustainability 14 (24), 16549.

Bosman, A., Casalbore, D., Anzidei, M., Muccini, F., Carmisciano, C., Chiocci, F.L., 2015. The first ultra-high resolution Digital Terrain Model of the shallow-water sector around Lipari Island (Aeolian Islands, Italy). Ann. Geophys. 58 (2), 1–11.

Capecchiacci, F., Tassi, F., Vaselli, O., Venturi, S., 2025. The 2021–2023 unrest of Vulcano Island volcanic system (Aeolian Islands, Italy): geochemical evidence from fumarolic gas discharges and well waters. Bull. Volcanol. 87 (3), 24.

Cartigny, M.J., Postma, G., Van den Berg, J.H., Mastbergen, D.R., 2011. A comparative study of sediment waves and cyclic steps based on geometries, internal structures and numerical modeling. Mar. Geol. 280 (1–4), 40–56.

Casalbore, D., Bosman, A., Romagnoli, C., Chiocci, F.L., 2017. Small-scale bedforms generated by gravity flows in the Aeolian Islands. A. In: Guillén, J., Acosta, J., Chiocci, F., Palanques, A. (Eds.), Atlas of Bedforms in the Western Mediterranean. Springer, Cham, pp. 287–292.

Casalbore, D., Romagnoli, C., Bosman, A., De Astis, G., Lucchi, F., Tranne, C.A., Chiocci, F.L., 2019. Multi-stage formation of La Fossa Caldera (Vulcano Island, Italy) from an integrated subaerial and submarine analysis. Mar. Geophys. Res. 40, 479–492.
Casalbore, D., Passeri, F., Tommasi, P., Verrucci, L., Bosman, A., Romagnoli, C., Chiocci, F.L., 2020. Small-scale slope instability on the submarine flanks of insular volcanoes: the case-study of the Sciara del Fuoco slope (Stromboli). Int. J. Earth Sci. 109 (8), 2643–2658.
Casalbore, D., Clare, M.A., Pope, E.L., Quartau, R., Bosman, A., Chiocci, F.L., Romagnoli, C., Santos, R., 2021. Bedforms on the submarine flanks of insular volcanoes: new insights gained from high resolution seafloor surveys. Sedimentology 68 (4), 1400–1438.
Casalbore, D., Di Traglia, F., Romagnoli, C., Favalli, M., Gracchi, T., Tacconi Stefanelli, C., Nolesini, T., Rossi, G., Del Soldato, M., Manzella, I., Cole, P., Casagli, N., Chiocci, F.L., 2022. Integration of remote sensing and offshore geophysical data for monitoring the short-term morphological evolution of an active volcanic flank: a case study from Stromboli Island. Remote Sens. 14 (18), 4605.
Casalbore, D., Di Traglia, F., Favalli, M., Fornaciai, A., Romagnoli, C., Civico, R., Ricci, T., Berardino, P., Borselli, L., Calabria, P., Calvari, S., Carlà, T., Casagli, N., Casu, F., Chiocci, F.L., De Cesare, W., De Luca, C., Del Soldato, M., Esposito, A.M., Esposito, C., Giudicepietro, F., Gracchi, T., Lanari, R., Macedonio, G., Monterroso, F., Natale, A., Nolesini, T., Perna, S., Petronelli, D., Rossi, G., Stefanelli, C.T., 2025. Very fast canyon formation and evolution along active volcanic flanks: a case from Stromboli Island. Geomorphology 109961.
Chang, Y.C., Mitchell, N., Quartau, R., Hübscher, C., Rusu, L., Tempera, F., 2022. Asymmetric abundances of submarine sediment waves around the Azores volcanic islands. Mar. Geol. 449, 106837.
Cicala, A., 2000. Guida alla meteorologia delle Isole Eolie. Lipari (Me) 1–150.
Clare, M.A., Yeo, I.A., Watson, S., Wysoczanski, R., Seabrook, S., Mackay, K., Hunt, J.E., Lane, E., Talling, P.J., Pope, E., Cronin, S., Ribó, M., Kula, T., Tappin, D., Henrys, S., de Ronde, C., Urlaub, M., Kutterolf, S., Fonua, S., Panuve, S., Veverka, D., Rapp, R., Kamalov, Williams, M., 2023. Fast and destructive density currents created by ocean-entering volcanic eruptions. Science 381 (6662), 1085–1092.
De Astis, G., Ventura, G., Vilardo, G., 2003. Geodynamic significance of the Aeolian volcanism (Southern Tyrrhenian Sea, Italy) in light of structural, seismological, and geochemical data. Tectonics 22 (4).
De Astis, G., Lucchi, F., Dellino, P., La Volpe, L., Tranne, C.A., Frezzotti, M.L., Peccerillo, A., 2013. Geology, volcanic history and petrology of Vulcano (central Aeolian archipelago). In: Lucchi, F., Peccerillo, A., Keller, J., Tranne, C.A., Rossi, P.L. (Eds.), The Aeolian Islands Volcanoes, Geological Society Memoirs, London, vol. 38, pp. 281–349.
De Astis, G., Doronzo, D.M., Di Vito, M.A., 2023. A review of the tectonic, volcanological and hazard history of Vulcano (Aeolian Islands, Italy). Terra Nova 35 (6), 471–487.
Di Traglia, F., Pistolesi, M., Rosi, M., Bonadonna, C., Fusillo, R., Roverato, M., 2013. Growth and erosion: the volcanic geology and morphological evolution of La Fossa (Island of Vulcano, Southern Italy) in the last 1000 years. Geomorphology 194, 94–107.
Di Traglia, F., Fornaciai, A., Casalbore, D., Favalli, M., Manzella, I., Romagnoli, C., Chiocci, F.L., Cole, P., Nolesini, T., Casagli, N., 2022. Subaerial-submarine morphological changes at Stromboli volcano (Italy) induced by the 2019–2020 eruptive activity. Geomorphology 400, 108093.
Di Traglia, F., Pistolesi, M., Bonadonna, C., Rosi, M., 2024. The last 1100 years of activity of La Fossa caldera, Vulcano Island (Italy): new insights into stratigraphy, chronology, and landscape evolution. Bull. Volcanol. 86 (5), 1–28.
Di Trapani, F.P., Di Maggio, C., Madonia, P., 2011. The role of volcanic and anthropogenic activities in controlling the erosional processes at Vulcano Island (Italy). Geogr. Fis. Din. Quat. 34 (1), 89–94.
Falsaperla, S., Spampinato, S., Cocina, O., Barreca, G., 2025. A 34-Year Record of Seismic Activity at Vulcano Island, Italy. https://doi.org/10.20944/preprints202501.2009.v1.
Federico, C., Cocina, O., Gambino, S., Paonita, A., Branca, S., Coltelli, M., Italiano, F., Bruno, V., Caltabiano, T., Camarda, M., Capasso, G., De Gregorio, S., Diliberto, I.S., Di Martino, R.M.S., Falsaperla, S., Greco, F., Pecoraino, G., Salerno, G., Sciotto, M., Bellomo, S., Di Grazia, G., Ferrari, F., Gattuso, A., La Pica, L., Mattia, M., Pisciotta, A. F., Pruiti, L., Sortino, F., 2023. Inferences on the 2021 ongoing volcanic unrest at Vulcano Island (Italy) through a comprehensive multidisciplinary surveillance network. Remote Sens. 15 (5), 1405.
Ferrucci, M., Pertusati, S., Sulpizio, R., Zanchetta, G., Pareschi, M.T., Santacroce, R., 2005. Volcaniclastic debris flows at La Fossa Volcano (Vulcano Island, southern Italy): insights for erosion behaviour of loose pyroclastic material on steep slopes. J. Volcanol. Geotherm. Res. 145 (3–4), 173–191.
Gabbianelli, G., Romagnoli, C., Rossi, P.L., Calanchi, N., Lucchini, F., 1991. Submarine morphology and tectonics of Vulcano (Aeolian Islands, Southern Tyrrhenian Sea). Acta Vulcanol. 1, 135–141.
Gambino, S., Laudani, A., Mangiagli, S., 2014. Seismicity pattern changes before the M = 4.8 Aeolian Archipelago (Italy) earthquake of August 16, 2010. Sci. World J. 2014 (1), 531212.
Geyer, A., Marti, J., 2008. The new worldwide collapse caldera database (CCDB): a tool for studying and understanding caldera processes. J. Volcanol. Geotherm. Res. 175 (3), 334–354.
Gvirtzman, Z., Nur, A., 1999. The formation of Mount Etna as the consequence of slab rollback. Nature 401 (6755), 782–785.
Hissmann, K., Rothenbeck, M., Wenzlaff, E., Weiß, T., Leibold, P., 2020. RV ALKOR Fahrtbericht/Cruise Report AL533-Mutual Field Trials of the Manned Submersible JAGO and the Hover-AUVs ANTON and LUISE off the Aeolian Islands, Mediterranean Sea, Catania (Italy)–La Seyne-sur-mer (France) 05.02.–18.02. 2020.
Inguaggiato, S., Vita, F., Diliberto, I.S., Mazot, A., Calderone, L., Mastrolia, A., Corrao, M., 2022. The extensive parameters as a tool to monitoring the volcanic activity: the case study of Vulcano Island (Italy). Remote Sens. 14 (5), 1283.
Lynett, P., McCann, M., Zhou, Z., Renteria, W., Borrero, J., Greer, D., Fa'anunu, O., Bosserelle, C., Jaffe, B., La Selle, S.P., Ritchie, A., Snyder, A., Nasr, B., Bott, J., Graehl, N., Synolakis, C., Ebrahimi, B., Cinar, G.E., 2022. Diverse tsunamigenesis triggered by the Hunga Tonga-Hunga Ha'apai eruption. Nature 609 (7928), 728–733.
Madonia, P., Liotta, M., 2010. Chemical composition of precipitation at Mt. Vesuvius and Vulcano Island, Italy: volcanological and environmental implications. Environ. Earth Sci. 61, 159–171.
Madonia, P., Cangemi, M., Olivares, L., Oliveri, Y., Speziale, S., Tommasi, P., 2019. Shallow landslide generation at La Fossa cone, Vulcano island (Italy): a multidisciplinary perspective. Landslides 16 (5), 921–935.
Malaguti, A.B., Rosi, M., Pistolesi, M., Speranza, F., Menzies, M., 2022. The contribution of palaeomagnetism, tephrochronology and radiocarbon dating to refine the last 1100 years of eruptive activity at Vulcano (Italy). Bull. Volcanol. 84, 1–19.
Mitchell, N.C., 2005. Interpreting long-profiles of canyons in the USA Atlantic continental slope. Mar. Geol. 214 (1–3), 75–99.
Ricciardi, A., Scalzo, A., Cristiani, C., Fiorito, D., Durantini, M., Colombi, A., Ciervo, M., Lombardo, E., Silvestri, M., Spatola, P., 2024. Emergency management and risk reduction measures during the Vulcano (Aeolian Islands) unrest 2021–2023. Bull. Volcanol. 86 (5), 42.
Romagnoli, C., Casalbore, D., Chiocci, F.L., 2012. La Fossa Caldera breaching and submarine erosion (Vulcano island, Italy). Mar. Geol. 303, 87–98.
Romagnoli, C., Casalbore, D., Bosman, A., Braga, R., Chiocci, F.L., 2013. Submarine structure of Vulcano volcano (Aeolian Islands) revealed by high-resolution bathymetry and seismo-acoustic data. Mar. Geol. 338, 30–45.
Romagnoli, C., Bosman, A., Casalbore, D., Anzidei, M., Doumaz, F., Bonaventura, F., Meli, M., Verdirame, C., 2022. Coastal erosion and flooding threaten low-lying coastal tracts at lipari (Aeolian islands, Italy). Remote Sens. 14 (13), 2960.
Rytuba, J.J., 1994. Evolution of volcanic and tectonic features in caldera settings and their importance in localization of ore deposits. Econ. Geol. 89 (8), 1687–1696.
Seabrook, S., Mackay, K., Watson, S.J., Clare, M.A., Hunt, J.E., Yeo, I.A., Lane, E.M., Clark, M.R., Wysoczanski, R., Rowden, A.A., Kula, T., Hoffmann, L.J., Armstrong, E., Williams, M.J., 2023. Volcaniclastic density currents explain widespread and diverse seafloor impacts of the 2022 Hunga Volcano eruption. Nat. Commun. 14 (1), 7881.
Slootman, A., Cartigny, M.J., 2020. Cyclic steps: review and aggradation-based classification. Earth Sci. Rev. 201, 102949.
Soutter, E.L., Kane, I.A., Hodgson, D.M., Flint, S., 2021. The concavity of submarine canyon longitudinal profiles. J. Geophys. Res.: Earth Surf. 126 (10), e2021JF006185.
Suárez-Arriaga, M.C., Bundschuh, J., Samaniego, F., 2014. Assessment of submarine geothermal resources and development of tools to quantify their energy potentials for environmentally sustainable development. J. Clean. Prod. 83, 21–32.
Sunamura, T., 2021. A model for wave abrasion on underwater bedrock, with an application to rapidly downwearing tephra cones adjacent to Surtsey Island in Iceland. Earth Surf. Process. Landf. 46 (8), 1600–1609.
Terry, J.P., Goff, J., Winspear, N., Bongolan, V.P., Fisher, S., 2022. Tonga volcanic eruption and tsunami, January 2022: globally the most significant opportunity to observe an explosive and tsunamigenic submarine eruption since AD 1883 Krakatau. Geosci. Lett. 9 (1), 24.
Tinti, S., Bortolucci, E., Armigliato, A., 1999. Numerical simulation of the landslide-induced tsunami of 1988 on Vulcano Island, Italy. Bull. Volcanol. 61, 121–137.
Tommasi, P., Graziani, A., Rotonda, T., Bevivino, C., 2007. Preliminary analysis of instability phenomena at Vulcano Island, Italy. In: Malheiro, Nunes (Ed.), Proceedings 2nd ISRM International Workshop on Volcanic Rocks, Ponta Delgada (Açores). Taylor&Francis Group, London, ISBN 978-0-415-45140-6, pp. 147–154.
Ventura, G., 2013. Chapter 2 kinematics of the Aeolian volcanism (Southern Tyrrhenian Sea) from geophysical and geological data. In: Lucchi, F., Peccerillo, A., Keller, J., Tranne, C.A., Rossi, P.L. (Eds.), The Aeolian Islands Volcanoes, Vol 38, Geological Society Memoirs, London, vol. 37(1), pp. 3–11.
Ventura, G., Vilardo, G., Milano, G., Pino, N.A., 1999. Relationships among crustal structure, volcanism and strike–slip tectonics in the Lipari–Vulcano volcanic complex (Aeolian Islands, Southern Tyrrhenian Sea, Italy). Phys. Earth Planet. Inter. 116 (1–4), 31–52.
Williams, R., 2012. DEMs of difference. Geomorphological. Techniques 2 (3.2).

Web references

http://www.emodnet-bathymetry.eu (accessed on November 2025).
http://www.sias.regione.sicilia.it (accessed on November 2025).